Relative Intensity Calibration of the DIII-D Charge-Exchange Recombination Spectroscopy System Using Neutral Beam Injection into Gas[a)]

B.A. Grierson,[1, b)] K.H. Burrell,[2] C. Chrystal,[2] and S.R. Haskey[1]
[1)] *Princeton Plasma Physics Laboratory, Princeton University, Princeton, NJ 08543, USA*
[2)] *General Atomics, P.O. Box 85608, San Diego, CA 92186-5608, USA*

(Dated: 13 April 2018)

A new calibration method for the DIII-D charge-exchange spectroscopy system produces a smoother impurity density profile compared to previous techniques, improving the accuracy of the impurity density profile reconstruction. The relative intensity calibration between the chords of the DIII-D charge-exchange recombination (CER) spectroscopy system is performed by firing neutral beams into the evacuated vacuum vessel pre-filled with neutral gas. Relative calibration is required in order to account for uncertainty in the 3D geometry of the neutral beam. Previous methods using helium gas have been improved by using xenon, which emits an emission line close to the commonly used carbon wavelength 5290.5 A, as well as improved timing of the gas injection, inclusion of variations in the vessel pressure, and timing of neutral beam injection. Photoemission recorded by 112 sightlines viewing 6 neutral beams are compared and used to form a relative calibration factor for each sightline. This relative calibration is shown to improve the quality of the measured ion density profile.

I. INTRODUCTION

Magnetic fusion experiments equipped with neutral beam injection use active charge-exchange recombination (CER) spectroscopy[1,2] to deduce spatially resolved profiles of plasma and magnetic quantities[3]. Some of the key plasma quantities obtained by CER spectroscopy are the impurity and main-ion densities. Accurate impurity density measurements are required to construct the plasma profiles for many types of analysis such as equilibrium reconstruction and thermal, particle and momentum transport studies.

Determination of the plasma ion density is more challenging than the temperature and velocity obtained through spectral fitting because the entire optical system, consisting of mirrors, lenses, fiber optic cables, spectrometer and detector, must be absolutely calibrated. In principle, one could determine the photoemission throughput of each optical component individually, but in practice it is much more convenient to perform a complete assembly, and then calibrate the entire system as a whole. This has the advantage of producing a single absolute calibration factor for each sightline, but the disadvantage that optical components cannot be replaced during an experimental campaign. On DIII-D, this absolute calibration procedure is performed by using an integrating sphere (LabSphere) placed at the point of intersection where the neutral beam and sightline cross, as seen in Fig. 1, filling the optics in the same manner as during tokamak operations. Once the system is absolutely calibrated, applying the absolute calibration factor to each optical sightline together with knowledge of the sightline and neutral beam geometry, the ion density can be determined. In practice, this procedure tends to produce an ion density profile that is not spatially smooth, but suffers from systematic channel-to-channel variation. This is due to imperfect knowledge of the exact path length that the sightline takes through a diverging neutral beam. In order to correct for channel-to-channel systematic errors and produce a measured density profile that is smooth in space, a relative intensity calibration can be performed by firing the neutral beams into the gas filled tokamak, and arrive at a geometrical factor that serves as a correction. Similar techniques have been documented on other tokamaks such as JET[4].

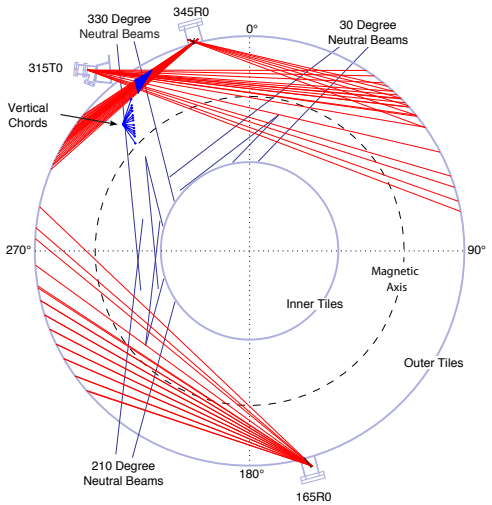

FIG. 1. DIII-D CER system displaying neutral beams, tangential and vertically viewing sightlines.

On the DIII-D tokamak the CER system consists of 112 sightlines that view six of the eight heating neu-

[a)] Contributed paper published as part of the Proceedings of the 22nd Topical Conference on High-Temperature Plasma Diagnostics, San Diego, CA, April, 2018.
[b)] Electronic mail: bgriers@pppl.gov

tral beam lines. The sightlines include views dedicated to impurity measurements that are horizontal and tangential to the axis of symmetry, vertically viewing from the bottom and the top of the machine, as well as dedicated main-ion viewing sightlines that are also tangential, but displaced in elevation below the tangential impurity views. Presented in this article is the procedure that has been used to produce an absolute and relative calibration of this diagnostic system. Previous[5] use of helium as the fill gas and recording the photoemission of the He-I line at 4686 Å has been replaced with the use of xenon for the spring 2014 experimental campaign and beyond. This is shown to improve the accuracy of the relative calibration for determining the carbon density profile by performing the calibration at the carbon wavelength, rather than performing the calibration at the helium wavelength and transferring that calibration to another spectral region. The procedure for applying this technique and the resulting improvement in the measured ion density profile is shown.

II. MODEL EQUATIONS

The DIII-D CER system currently uses high speed, actively cooled low noise CCD cameras for recording the photoemission spectrum. Fundamentally, the measurement is the number of digitizer counts produced by photoelectrons recorded across one dimension of the CCD chip. The process that produces the measured spectrum is the charge-exchange reaction in the core of the tokamak between the beam neutral n_b and plasma ion n_i with reaction rate $q_{CX}(v_b)$, where the rate is a function of the beam velocity of each neutral species at the full, half and third acceleration energy. Further, some sightlines cross multiple beams, and hence when both beams are on the contributions are added linearly. Photons are collected along a line of sight that passes through the beam volume, collecting the local emissivity. An expression[1,5] for the total photoemission ϕ^l collected by the optical system in units (ph/s/m^2/sr) for a given sightline l is given by Eq. 1 where j indicates beam species and k indicates beamline.

$$\phi^l = \frac{1}{4\pi}\int dl \sum_{j,k} n^j_{b,k}\ n_i\ q_{CX}(v^j_b) \tag{1}$$

Since the sightlines pass through the neutral beam in a relatively small volume tangential to flux surfaces, we can assume that the ion density is constant in this volume, and use a computation of the neutral beam attenuation to compute n^j_b to solve Eq. 1 for n_i. However, because n_b is a three dimensional object that would be expensive to compute quickly, we make a further assumption that the neutral beam is well described by an analytic form for an ideal diverging gaussian beam, given by Eq. 2.

$$\begin{aligned} n^j_b(x,y,z) &= \frac{n^j_{b_0}\ \zeta^j(z)}{\pi w_x(z) w_y(z)} \\ &\quad \times \exp\left[-\left(\frac{x}{w_x(z)}\right)^2 - \left(\frac{y}{w_y(z)}\right)^2\right] \\ w_x(z) &= w_x(z_0) + z\tan(\gamma_x) \\ w_y(z) &= w_y(z_0) + z\tan(\gamma_y) \end{aligned} \tag{2}$$

This reduces the neutral beam deposition calculation to be one-dimensional, often called a 'pencil' or 'filament' beam calculation. Here n_{b_0} is the 'pencil' density where the beam enters the vessel obtained from the power $P = e n_{b_0} v_b A_b E_{inj}$ where e is electron charge, v_b is the beam velocity, A_b is the beam cross-sectional area and E_{inj} is the injector energy. Attenuation $\zeta(z)$ is given by a dimensionless function of z along the beam, which is equal to one at the location that the beam enters the vessel and attenuates exponentially as the beam penetrates the plasma. Parameterization of the beam shape is give by the Gaussian width in the horizontal $w_y(z)$ and vertical $w_z(z)$ directions with divergence angles γ_x and γ_y, respectively. In the expression for the widths, z_0 is a reference distance from the ion source beyond which the beam is well represented by a Gaussian shape, typically taken as the location where the beam enters the vacuum vessel. These parameterizations of the beam shape are obtained from the monte-carlo neutral beam attenuation code NUBEAM[6] in TRANSP[7,8], and post-processed through the OMFIT[9] TRANSP module[10]. Shown in Fig. 2 is the simulation of the DIII-D beam 30LT with rectangular 5 cm source half-width and 24 cm source half-height. Divergence of the beam rays at the source is set at 8.73e-3 and 2.27e-2 radians in the horizontal and vertical directions, with infinity focus in the horizontal and 1000 cm focus in the vertical direction. By post-processing these simulation results the analytic parameters for the far-field optics can be derived, giving $w_x = 10.36$ cm and $w_y = 24.68$ cm for the horizontal and vertical widths of the beam where it enters the vessel. By computing the width along the beam deposition inside the tokamak, the slope of $w(z)$ provides $\gamma_x = 0.0123$ rad and $\gamma_y = 0.0358$ rad.

By using the parameterization for the beam neutral density in Eq. 2 in Eq. 1, we can rearrange the expression for the ion density measured by sightline l as

$$n^l_i = \sum_{j,k} \frac{4\pi\phi^l}{n^j_{b_0,k} q_{CX}(v^j_{b,k}) G^l_k} \tag{3}$$

where

$$G^l_k = \int dl \frac{n^j_{b,k}(x,y,z)}{n^j_{b_0}\zeta^j(z)} \tag{4}$$

is the 'geometry factor'. This geometry factor G^l_k is a scalar that is computed once for each beam numerically,

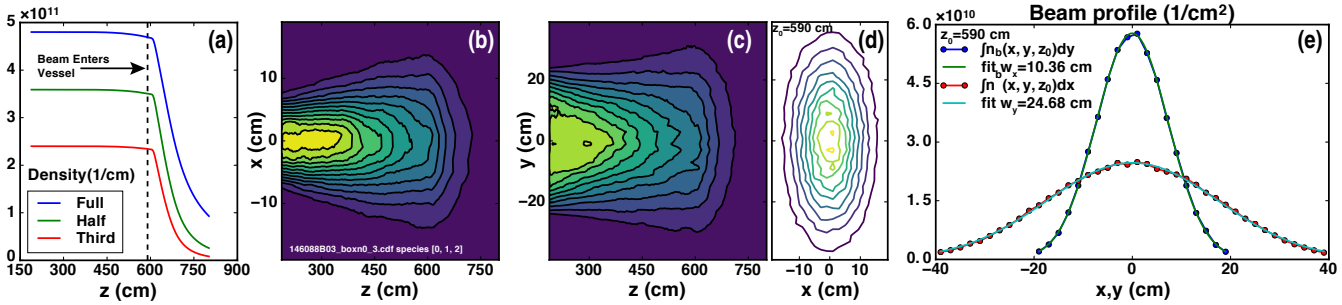

FIG. 2. Neutral beam injection from NUBEAM showing (a) the pencil density integrated over the cross-section, beam neutral density summed over species from (b) top-down projection, (c) side projection, (d) footprint and (e) beam profiles where the beam enters the vessel.

and then used in the computation of the ion density. For example, using the parameterization determined from the NUBEAM calculations shown in Fig. 2 and centrally viewing CER channel T01, we compute a geometry factor $G^{\mathrm{T01}}_{\mathrm{30LT}} = 3.02\ \mathrm{m}^{-1}$, which is within 5% of the historical value used for this channel.

In principle, the calibration is now complete and can be used to determine the plasma ion density. However, the knowledge of the 3D neutral beam geometry is incomplete for a number of reasons[11]. DIII-D's heating neutral beams are not all identical; 1) there are three different types of ion sources, 2) some of the beams have reduced aperture masking plates (RAMP) that narrow the ion source width, and 3) ion sources have been moved from one beamline to another during experimental campaigns, which transfers any source-specific features of the injection geometry. Further, measurements of the vertically diverging neutral beam shape is available on the most well-diagnosed (30LT) of the heating beams[12,13], but neither the horizontal divergence nor images of the other beams are readily available. These considerations motivate an *in-situ* relative calibration of all sources.

The 'beam-into-gas' relative intensity calibration is based on a single guiding principle: The gas density is constant throughout the vessel and there is no beam attenuation. Therefore all sightlines must measure the same gas density if there is negligible neutral beam attenuation and the gas density is constant in time. By taking Eq. 3 for a background gas n_g rather than plasma ion density, and setting it equal for two sightlines without any time-overlap in the beam injection, we arrive at the following expression:

$$G^{l}_{k} = \frac{\phi_k}{\phi^{l_0}_{k_0}} \frac{n_{b_0,k_0}}{n_{b_0,k}} G^{l_0}_{k_0} \tag{5}$$

where k_0 denotes reference beam and l_0 denotes reference sightline, which has historically been channel T01 viewing neutral beam 30LT. This expression permits the determination of the empirical geometry factor for all chords leveraging the accuracy of the geometry for a single chord-beam pair, which now embodies all of the systematic errors of the system.

III. BEAM-INTO-GAS AND RESULTS

Essential elements for the application of the beam-into-gas calibration are the monitoring of the vessel fill pressure during neutral beam injection and isolation of a clean spectrum near the wavelength of interest. The procedure for executing the beam-into-gas injection has been improved from the previous technique by

- First performing a data acquisition with only the gas injection and pressure monitors enabled. This determines the evolution of the background gas density $n_g(t)$ in time to augment Eq.5 by a factor $p_{g,k_0}/p_{g,k}$, which uses the vessel pressure gauge time history during injection of beam k.

  This is shown in Fig. 3(b), where it is clear that the neu- tral beam injection perturbs the vessel pressure (#172587). The evolution of the partial pressure of xenon underlying the total pressure is smoother in time and mildly decaying during the injection of the six beams, as seen by the no-beam reference (#172538)

  The evolution of the partial pressure of xenon is smoother in time and mildly decaying during the injection of the six beams.

$$G^{l}_{k} = \frac{\phi_k}{\phi^{l_0}_{k_0}} \frac{n_{b_0,k_0}}{n_{b_0,k}} \frac{p_{g,k_0}}{p_{g,k}} G^{l_0}_{k_0} \tag{6}$$

- During the neutral beam injection the injected power calculation for the DIII-D neutral beams has been upgraded to use the dynamic evolution of the current during the power turn-on, which modifies the perveance and transmitted power during a pulse. The power used in forming n_{b_0} in Eq. 5 is the reported time-dependent power over the integration period of the CCD camera, rather than time-independent scalars.

Spectroscopic data collected during the 50 ms long neutral beam pulses for helium and xenon gas are shown in Fig. 4 and Fig. 5, respectively. It can be seen that both spectra are relatively clean, with isolated lines near the

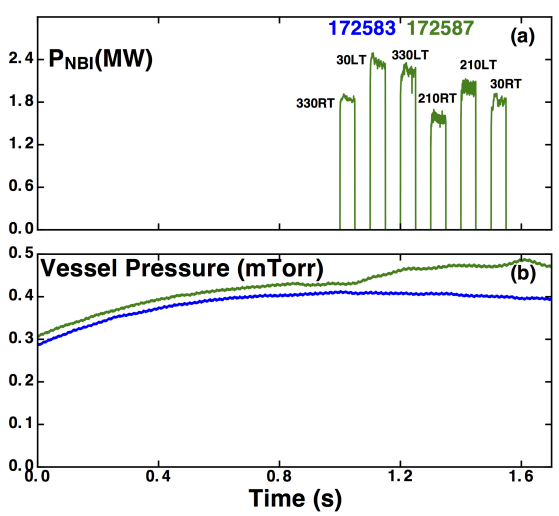

FIG. 3. Time evolution of (a) the neutral beam power and (b) the vessel pressure during the no-beam gas puff and the with-beam gas puff.

center of the CCD tuned to the respective wavelengths. Some time evolution in the spectrum can be seen, due to the dynamic power during the beam turn-on[13]. Relative geometry factors are computed for all sightlines using gaussian fits to the isolated spectral line near the center of each CCD camera and stored for routine data processing.

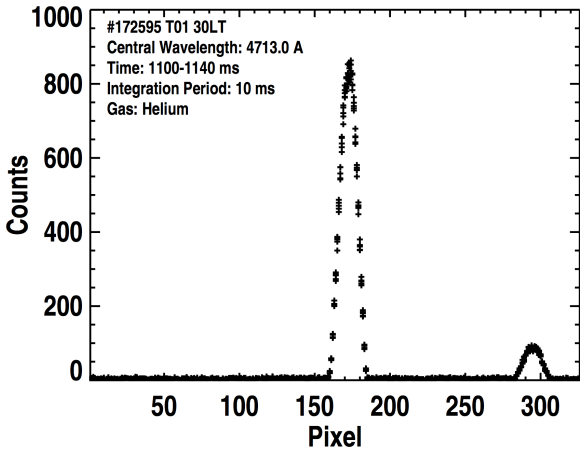

FIG. 4. Active helium spectrum from beam-into-gas.

Having completed the beam-into-gas relative calibration with the previously used helium and new xenon measurements, we compute the carbon impurity density profiles produced by the beam-into-gas calibration using helium gas near the 4686 Å helium charge-exchange wavelength, with the calibration using xenon gas near the carbon 5290.5 Å wavelength. Shown in Fig. 6 is the comparison of two carbon density profiles that are produced by the two different calibration techniques. First, Fig. 6(a) shows the carbon density using the helium beam-into-gas and neglecting time dependence of the background gas density and dynamic evolution of the neutral beam power. There are systematic differences between the various viewing systems that view separate beams, and appear to produce separate profiles, which may be linked to the optical elements or spectrometer intensity response with wavelength common to entire sub-systems. For these reasons, impurity transport experiments have typically performed analysis using only one spectroscopic system viewing one neutral beam in order to eliminate beam-to-beam systematic variations in the measured profile. Second, in Fig. 6(b) we apply the new calibration technique using xenon gas at the same wavelength as the commonly measured carbon ions; we see significant reduction in the amount of scatter and systematic offsets. There are a number of potential reasons for the difference in the profiles produced by the two calibration procedures. Some potential reasons are the variation in the throughput and quality of absolute calibration between the two wavelength regions, spectrometer dispersion, and scattered light. However none of these possibilities have been conclusively identified. Future efforts to improve the calibration further across the entire visible spectrum are being considered, due to the commonly use of CER for study of other impurities such as helium, lithium, nitrogen, fluorine, neon, aluminum and argon.

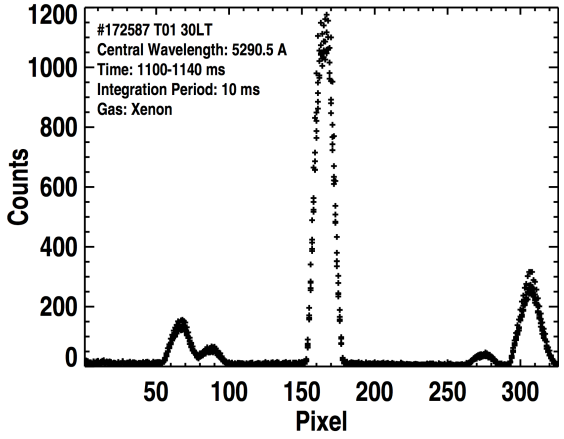

FIG. 5. Active xenon spectrum from beam-into-gas.

ACKNOWLEDGMENTS

We acknowledge use of the Atomic Data and Analysis Structure (ADAS) database in the analysis of the impurity density. The originating developer of ADAS is the JET Joint Undertaking. This work supported in part by the the U.S. Department of Energy under DE-FC02-04ER54698, DE-AC02-09CH11466. The author gratefully acknowledges useful discussions with W.M. Solomon, W.W. Heidbrink and M.A. Van Zeeland.

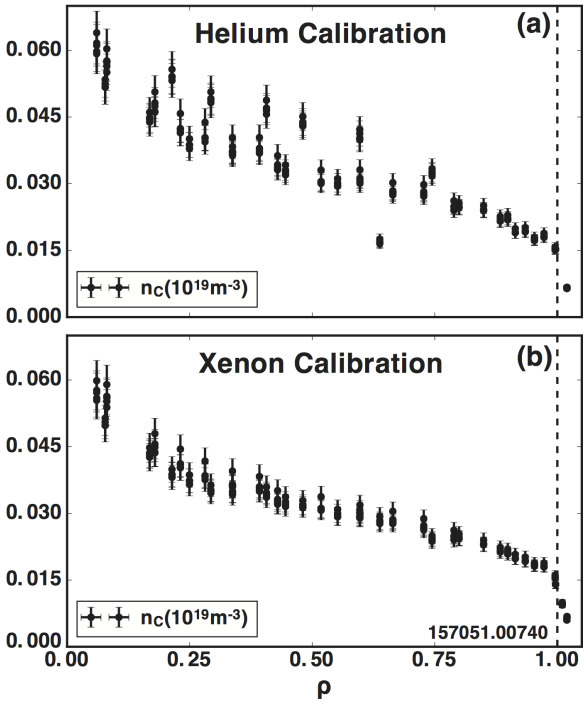

FIG. 6. Comparison of carbon impurity density using the beam into gas calibration from (a) helium gas and (b) xenon gas.

[1] Fonck, D. Darrow, and K. Jaehnig, Physical Review A **29**, 3288 (1984).
[2] R. Isler, Plasma Physics and Controlled Fusion **36**, 171 (1994).
[3] D. M. Thomas, G. R. Mckee, K. H. Burrell, F. Levinton, E. L. Foley, and R. K. Fisher, Fusion science and technology **53**, 487 (2008).
[4] C. Giroud, A. G. Meigs, C. R. Negus, K.-D. Zastrow, T. M. Biewer, T. W. Versloot, and J. E. Contributors, Review of Scientific Instruments **79**, 10F525 (2008).
[5] D. F. Finkenthal, Doctoral Dissertation , 1 (1994).
[6] A. Pankin, D. McCune, R. Andre, G. Bateman, and A. H. Kritz, Computer Physics Communications **159**, 157 (2004).
[7] R. J. Hawryluk, Course on Physics of Plasmas Close to Thermonuclear Conditions , 1 (1979).
[8] R. Goldston, D. McCune, H. Towner, S. Davis, R. J. Hawryluk, and G. Schmidt, Journal of Computational Physics **43**, 61 (1981).
[9] O. Meneghini, S. P. Smith, L. L. Lao, O. Izacard, Q. Ren, J. M. Park, J. Candy, Z. Wang, C. J. Luna, V. A. Izzo, B. A. Grierson, P. B. Snyder, C. Holland, J. Penna, G. Lu, P. Raum, A. McCubbin, D. M. Orlov, E. A. Belli, N. M. Ferraro, R. Prater, T. H. Osborne, A. D. Turnbull, and G. M. Staebler, Nuclear Fusion **55**, 083008 (2015).
[10] B. A. Grierson, X. Yuan, M. Gorelenkova, S. M. Kaye, N. C. Logan, O. Meneghini, S. R. Haskey, J. Buchanan, M. Fitzgerald, S. P. Smith, L. Cui, R. V. Budny, and F. M. Poli, Fusion science and technology (2018).
[11] C. Chrystal, K. H. Burrell, B. A. Grierson, and D. C. Pace, Review of Scientific Instruments **86**, 103509 (2015).
[12] M. A. Van Zeeland, Plasma Physics and Controlled Fusion **52**, 1 (2010).
[13] B. A. Grierson, K. H. Burrell, B. Crowley, L. R. Grisham, and J. T. Scoville, Review of Scientific Instruments **85**, 103502 (2014).